Oncogenes and Tumor Suppressors

Molecular Cancer Research

The mTOR Targets 4E-BP1/2 Restrain Tumor Growth and Promote Hypoxia Tolerance in PTEN-driven Prostate Cancer

Mei Ding[1], Theodorus H. Van der Kwast[2], Ravi N. Vellanki[1], Warren D. Foltz[3,4], Trevor D. McKee[1,3], Nahum Sonenberg[5], Pier P. Pandolfi[6], Marianne Koritzinsky[1,4,7], and Bradly G. Wouters[1,4,8,9]

Abstract

The mTOR signaling pathway is a central regulator of protein synthesis and cellular metabolism in response to the availability of energy, nutrients, oxygen, and growth factors. mTOR activation leads to phosphorylation of multiple downstream targets including the eukaryotic initiation factor 4E (eIF4E) binding proteins-1 and -2 (EIF4EBP1/4E-BP1 and EIF4EBP2/4E-BP2). These binding proteins inhibit protein synthesis, but are inactivated by mTOR to stimulate cell growth and metabolism. However, the role of these proteins in the context of aberrant activation of mTOR, which occurs frequently in cancers through loss of PTEN or mutational activation of the PI3K/AKT pathway, is unclear. Here, even under conditions of aberrant mTOR activation, hypoxia causes dephosphorylation of 4E-BP1/4E-BP2 and increases their association with eIF4E to suppress translation. This is essential for hypoxia tolerance as knockdown of 4E-BP1 and 4E-BP2 decreases proliferation under hypoxia and increases hypoxia-induced cell death. In addition, genetic deletion of 4E-BP1 and 4E-BP2 significantly accelerates all phases of cancer development in the context of PTEN loss–driven prostate cancer in mice despite potent PI3K/AKT and mTOR activation. However, even with a more rapid onset, tumors that establish in the absence of 4E-BP1 and 4E-BP2 have reduced levels of tumor hypoxia and show increased cell death within hypoxic tumor regions. Together, these data demonstrate that 4E-BP1 and 4E-BP2 act as essential metabolic breaks even in the context of aberrant mTOR activation and that they are essential for the creation of hypoxia-tolerant cells in prostate cancer. *Mol Cancer Res; 16(4); 682–95. ©2018 AACR.*

Introduction

The microenvironment of human tumors is characterized by extreme heterogeneities in oxygen levels, driven by dynamic changes in oxygen delivery and cellular metabolism (1). Hypoxic cancer cells become resistant to conventional cancer treatment including both radiotherapy and chemotherapy and are associated with more aggressive disease and poor prognosis. In prostate cancer, hypoxia is associated with poor overall outcome and more rapid failure following primary treatment with radiotherapy or surgery (2). Several independent signaling pathways that respond to hypoxia and influence hypoxia tolerance and metabolism have been identified (3). These include potent transcriptional responses driven in part by the HIF (hypoxia inducible factor) family of transcription factors that promote changes in cellular metabolism, oxygen consumption, and induction of angiogenesis (4). In addition, we and others have demonstrated that hypoxia influences gene expression and cell phenotype through pathways that regulate mRNA translation through signaling changes driven by two other key oxygen-sensitive signaling pathways—the unfolded protein response (UPR) and mTOR (5, 6). Hypoxia (0%–0.2% O_2) causes a rapid inhibition of mRNA translation (5) with kinetics that precede ATP deletion and results from signaling through both UPR and mTOR pathways (7–9).

Initial inhibition of translation during hypoxia occurs downstream of UPR signaling induced by endoplasmic reticulum (ER) stress due to suppression of disulfide bond formation (10), and inhibition of the initiation step of mRNA translation through PERK-dependent phosphorylation of eIF2α. Prolonged mRNA translation inhibition during hypoxia (8–24 hours) occurs independently of eIF2α and is due instead to suppression eukaryotic initiation factor 4E (eIF4E) and cap-dependent translation initiation. eIF4E is a rate-limiting protein that is required for the initiation step of protein synthesis through binding to the 7-methyl-guanosine 5′ cap of cellular mRNAs. eIF4E associates with eIF4G (ATPase) and eIF4A (RNA helicase) to form eIF4F at the 5′ cap and initiate protein synthesis. Suppression of cap-dependent

[1]Princess Margaret Cancer Centre and Campbell Family Institute for Cancer Research, University Health Network, Toronto, Ontario, Canada. [2]Department of Pathology, University Health Network, Toronto, Ontario, Canada. [3]Radiation Medicine Program, Princess Margaret Cancer Centre, University of Toronto, Toronto, Ontario, Canada. [4]Department of Radiation Oncology, University of Toronto, Toronto, Ontario, Canada. [5]Department of Biochemistry and Goodman Cancer Research Centre, McGill University, Montreal, Quebec, Canada. [6]Cancer Research Institute, Beth Israel Deaconess Cancer Center, Department of Medicine and Pathology, Beth Israel Deaconess Medical Center, Harvard Medical School, Boston, Massachusetts. [7]Institute of Medical Science, University of Toronto, Toronto, Ontario, Canada. [8]Ontario Institute for Cancer Research, Toronto, Ontario, Canada. [9]Department of Medical Biophysics, University of Toronto, Toronto, Ontario, Canada.

Note: Supplementary data for this article are available at Molecular Cancer Research Online (http://mcr.aacrjournals.org/).

Corresponding Author: Bradly G. Wouters, Princess Margaret Cancer Centre and University Health Network, University of Toronto, 1-S-407, R. Fraser Elliott Building, 200 Elizabeth Street, Toronto, Ontario M5G 2C4, Canada. Phone: 416-340-4407; Fax: 416-581-7840; E-mail: brad.wouters@uhnresearch.ca

doi: 10.1158/1541-7786.MCR-17-0696

protein synthesis during hypoxia is due to reduced phosphorylation of eukaryotic initiation factor 4E binding proteins (4E-BP), which bind to eIF4E in their under phosphorylated form and prevent its association with eIF4G at the 5′ cap (11, 12). In mammals, there are three members in 4E-BP family—4E-BP1, 4E-BP2, and 4E-BP3 (13). All three corresponding proteins are believed to negatively regulate eIF4E; however, only 4E-BP1and 4E-BP2 have been shown to be regulated in a similar manner and expressed in most tissues, although 4E-BP2 is particularly high in brain (14). The ability of 4E-BP1 and 4E-BP2 to bind and inhibit eIF4E is prevented by mTOR-dependent phosphorylation on a number of sites (15). Consequently, mTOR inhibition during hypoxia leads to reduced phosphorylation of these proteins and consequential inhibition of eIF4E and cap-dependent translation (5).

The mTOR signaling pathway is a central regulator of cellular metabolism and is influenced by many upstream signaling pathways in response to the availability of nutrients and growth factors. mTOR signaling regulates cell growth and survival in response to PI3K/AKT signaling by controlling multiple anabolic processes including rates and capacity of protein synthesis and mitochondrial activity (16, 17). As such, it functions in part as a central coordinator of energy production and expenditure. Stimulation of protein synthesis occurs through mTOR increases in ribosome biogenesis, and direct phosphorylation of p70S6K (ribosomal protein S6 kinase), 4E-BPs and eEF2K (eukaryotic elongation factor 2), resulting in increased rates of initiation and elongation, and increased capacity of mRNA translation.

Aberrant activation of the PI3K/AKT/mTOR signaling pathway through loss of the tumor suppressor PTEN protein or mutations in proteins in the PI3K/AKT pathway are extremely common in prostate and other types of cancer. Because eIF4E levels are rate limiting, phosphorylation of 4E-BPs during aberrant mTORC1 activation in cancer is a strong inducer of cap-dependent translation. Consequential activation of mTOR signaling and increased activity of eIF4E cap-dependent translation is thought to be a critical mediator of its role in tumorigenesis. Indeed, it has shown in mouse models of prostate cancer that knock-in mice expressing a nonphosphorylatable form of eIF4E are resistant to tumorigenesis. Overexpression of eIF4E (eukaryotic initiation factor 4E) is found frequently in cancer, and has been shown to cooperate with other driver mutations like Kras to stimulate transformation (18–22). Similarly, aberrant activation of eIF4E through dual knockout of 4E-BP1 and 4E-BP2 has been shown to increase tumorigenesis in p53 knockout mice (23).

The importance and role of the 4E-BPs in the context of aberrant mTOR signaling and hypoxia in cancer has not been explored. Our previous data demonstrate that 4E-BPs play a critical role in mediating a stress response to hypoxia. We hypothesize that their ability to inhibit translation during conditions of such extreme nutrient deprivation is critical to survival. We have shown that partial knockdown of 4E-BP1 resulted in loss of hypoxia tolerance and a reduction in the hypoxia observed in U87 glioblastoma xenografts in mice (24). Here, we have investigated the consequences of genetic loss of 4E-BP1 and 4E-BP2 in the context of PTEN-driven models of prostate cancer. Our data reveal that through loss of these regulators, mRNA translation accelerates tumorigenesis even in the context of PTEN loss, and the tumors that arise show substantial reductions in their ability to tolerate hypoxia.

Materials and Methods

Generation of transgenic mice

All animal experimentation was conducted in accordance with the Canadian Guide for the Care and Use of Laboratory Animals, and protocols were approved by the Animal Care Committee at the Princess Margaret Hospital Cancer Center, University Health Network, University of Toronto (Toronto, Ontario, Canada). The Probasin-Cre mouse line expresses Cre-recombinase transcript under control of mouse prostate epithelial-specific probasin promoter. The $Pten^{flox/flox}$ mice and Probasin-Cre mice were kindly provided by Dr. Pier P. Pandolfi's laboratory (25). Mouse lines with 4E-BP1 and 4E-BP2 knockout were kindly provided by N. Sonenberg's laboratory (26). To generate mice with prostate epithelial-specific *Pten* gene deletion, $Pten^{flox/flox}$ mice were bred to probasin-Cre mice. To generate mice carrying Pten deletion in 4E-BP1 and 4E-BP2 knockout background, $Pten^{flox/flox}$/Probasin-Cre mice were bred to 4E-BP1 and 4E-BP2 knockouts. After several breedings, mice carrying all four transgenes ($Pten^{flox/flox}$, probasin-Cre, 4EBP1 and 4EBP2 knockout) were obtained. Genotypes were confirmed by PCR.

The genetic background strain for $Pten^{flox/flox}$ mice and 4EBP1/2 knockouts is C57/Black 6, and for Probasin-Cre mice is mixed. Littermates were used for all comparisons and analyses.

Genotype analysis

Genomic DNA from tails of 3 weeks of age transgenic mice was isolated and used for genotypic PCR analysis as described previously (25, 26).

Histologic and pathologic analysis

Transgenic mouse prostates were dissected, fixed in 10% formalin in PBS, and embedded in paraffin. Sections (4-μm thick) were cut and stained with hematoxylin and eosin (H&E), examined, and photographed with a Leica camera DFC 320 and Leica DMLB microscope (Leica Microsystems).

EF5 administration

To identify hypoxia regions of the prostate tumor, mice received an injection of the hypoxia marker drug EF5 [2-(2-nitor-1H-imidazole-1-yl)-N-(2,2,3,3,3-pentafluoropropyl)acetamide], 3 hours before tumor excision (27). To achieve optimal drug distribution and tumor staining, each mouse received a total body dose of 10 μL/g i.p. of a 10 mmol/L EF5 in 2.4% EtOH, 5% dextrose.

Immunostaining analysis (IHC)

Prostate tissue was fixed in 10% formalin and embedded in paraffin, and 4-μm thick sections were prepared. Primary antibodies used were: phospho-4E-BP1 1:50 dilutions (Cell Signaling Technology), 4E-BP2 1:100 dilutions (Cell Signaling Technology), phospho-eIF4E 1:500 dilutions (BD Biosciences). IHC for detection of tumor vasculature was achieved by staining CD31 antibody, 1:500 dilution (Santa Cruz Biotechnology), respectively. Apoptosis was assessed using caspase-3 antibody, 1:200 dilution (Cell Signaling Technology) and hypoxia was assessed using an EF5 antibody, 1:150 dilution (provided by Dr. Cameron Koch, University of Pennsylvania, Philadelphia, PA) in caspase-3 and EF5 double immunostaining. Images with EF5 staining (red), caspase-3 (green), and DAPI counterstain (blue) were obtained from immunofluorescence-stained slides

digitized at 1-μm/pixel resolution on a Huron Technologies TissueScope scanner. Image analysis was performed on Definiens TissueStudio software, in which 5–7 representative regions were segmented to separate prostate tumor from lumen, and prostate tumor regions were quantified to identify the number of positively stained EF5 cells, caspase-3 cells and EF5/caspase coexpressed cells as a percentage of the total cells in the tumor region.

MRI analysis

MR images to visualize morphologic changes in the murine genitourinary region over time were acquired using a 7 Tesla preclinical MRI system (Biospec 70/30, Bruker Corporation), equipped with a B-GA12 gradient coil insert, 7.2-cm inner diameter linearly polarized RF volume coil, and 4-coil phased-array surface receiver coil. Mice were anaesthetized and maintained at 1.8% isoflurane delivered via nose cone, and respiration was monitored using a pneumatic pillow (SA Instruments). Imaging was then performed with mice oriented in prone position above the posteriorly placed phased-array coil. The prostate gland and genitourinary region was resolved using a stack of 2D T2-weighted Rapid Acquisition with Refocused Echoes (RARE) images with echo time 48 ms, repetition time 4,200 ms, and spatial resolution of at least $0.13 \times 0.13 \times 1$ mm. Slice thickness increased from 0.5 to 1 mm during the course of the study to encompass the enlarging prostate volume, and scan times were then correspondingly reduced from 15 to 8 minutes given higher signal-to-noise in thicker slice acquisitions.

Cell cultures

HCT116, DU145, PC3, and LNCAP cell lines were obtained from ATCC. Cell line authenticity was confirmed by short tandem repeat (STR) profiling every 2 months and cell lines were also checked for mycoplasma contamination at the same frequency. All cell lines were grown in RPMI supplemented with 10% FBS. Viral particles from pLKO.1 shRNA knockdown vectors were produced as described previously (28). 4E-BP1 shRNA target sequence is GCCAGGCCTTATGAAAGTGAT. 4E-BP2 shRNA target sequence is CTCGAATCATTTATGACAGAA. For hypoxic exposure, cells were seeded 24 hours prior to transfer to a hypoxia culture chamber (MACS VA 500 microaerophilic workstation, Don Whitley Scientific).

Western blotting

Primary antibodies were used at the following dilutions: 4E-BP1 1:1,000 (Cell Signaling Technology), 4E-BP2 1:1,000 (Cell Signaling Technology), phosphor 4E-BP1 T37/46 1:1,000 (Cell Signaling Technology), phosphor 4E-BP1 S65 1:1,000 (Cell Signaling Technology). eIF4E 1:1,000 (BD Biosciences), β-actin 1:10,000 (MP Biomedicals). HRP-secondary rabbit antibody was used at 1:5,000 dilutions (GE Healthcare). Experiments were performed a minimum of three times.

Immunoprecipitation

Cells were lysed and protein was extracted with lysis buffer (5 mmol/L HEPES-KOH pH 7.5, 150 mmol/L KCl, 1mmol/L EDTA pH 8.0, 2 mmol/L DTT, 0.2% Tween-20). Four-hundred micrograms of extracted protein was incubated with 50 μL of 7-methyl-GTP sepharose resin (GE Healthcare) overnight at 4°C. The resin was washed, boiled in Laemmli buffer, and the polypeptides in the supernatant were resolved on a large gradient SDS-PAGE, transferred to nitrocellulose membrane and immunoblotted. All experiments were performed in triplicate.

Clonogenic assay

Colony formation assays were performed in triplicate on the relevant cell lines in parallel, with appropriate controls following hypoxia (0.2%) exposure in 60-mm petri dishes as described previously (29).

Statistical analysis

Student *t* test (two-sided) was calculated using GraphPad Prism (GraphPad software, Inc.) to test for statistical differences. *P* values <0.05 were considered significant. The log-rank test was used to compare for statistically significant differences in cancer-free survival (Kaplan–Meier survival curve) and was performed using R version 3.0.1. A one-way ANOVA and Tukey method was calculated for Ki67 and CD31 immunostaining quantification. Mann–Whitney test and *t* test were used to evaluate the significance in comparison of different groups in EF5, caspase-3 immunostaining quantification.

Results

4E-BP1 and 4E-BP2 are dephosphorylated during hypoxia and inhibit eIF4F formation in human prostate cells

To evaluate the functional roles of 4E-BP1 and 4E-BP2 in hypoxia, we analyzed 4E-BP1 and 4E-BP2 levels during normoxia and hypoxia conditions at different time points in three human prostate cell lines with different genetic background—DU145, PC3, and LNCAP (Fig. 1A–C). DU145 and PC3 cells have both been reported to have loss of PTEN function and consequently mTOR activation. As shown previously, 4E-BP1 migrates as three different bands representing different phosphorylation levels with the fastest migrating band representing the dephosphorylated version (30). In DU145 cells (Fig. 1A), 4E-BP1 was substantially dephosphorylated during exposure to 0.2% O_2 at 24, 48, and 72 hours and exposure to 0% for 24 hours as evidenced by a loss of the slowest migrating band and a concomitant increase in the two higher mobility bands. Phosphorylation-specific 4E-BP1 antibodies for T37/46 and S65 confirmed the 4E-BP1 dephosphorylation during 24- to 72-hour exposure to 0.2% O_2. 4E-BP2 expression was weak at 72-hour exposure to 0.2% O_2 (Fig. 1A). In PC3 cells, 4E-BP1 was also dephosphorylated during exposure to 0.2% O_2 24- to 72 hours; however, there was no change in phosphorylation of 4E-BP1 S65 antibody and only mild dephosphorylation displayed during 72-hour exposure to 0.2% O_2 and 24-hour exposure to 0% O_2. There were no significant differences in 4E-BP2 expression during normoxia or hypoxia at different time points (Fig. 1B). In LNCAP cells, we saw similar evidence of 4E-BP1 dephosphorylation only after 0.2% O_2 for 72 hours or 0% O_2 for 24 hours (Fig. 1C). No change was observed at 24 or 48 hours of 0.2% O_2.

The assembly of the eIF4F complex for mRNA cap-dependent translation is the critical determinant of translation initiation. 4E-BPs competes with eIF4G for a common binding site to eIF4E and it is mutually exclusive. As 4E-BP dephosphorylation during hypoxia can increase binding to eIF4E, this can lead to eIF4E separation from eIF4G and disrupt eIF4F formation and cap-dependent translation. To further test the functional effects on 4E-BP dephosphorylation in DU145 and PC3 prostate cell lines during exposure to 0.2% O_2, immunoprecipitation (IP) methods

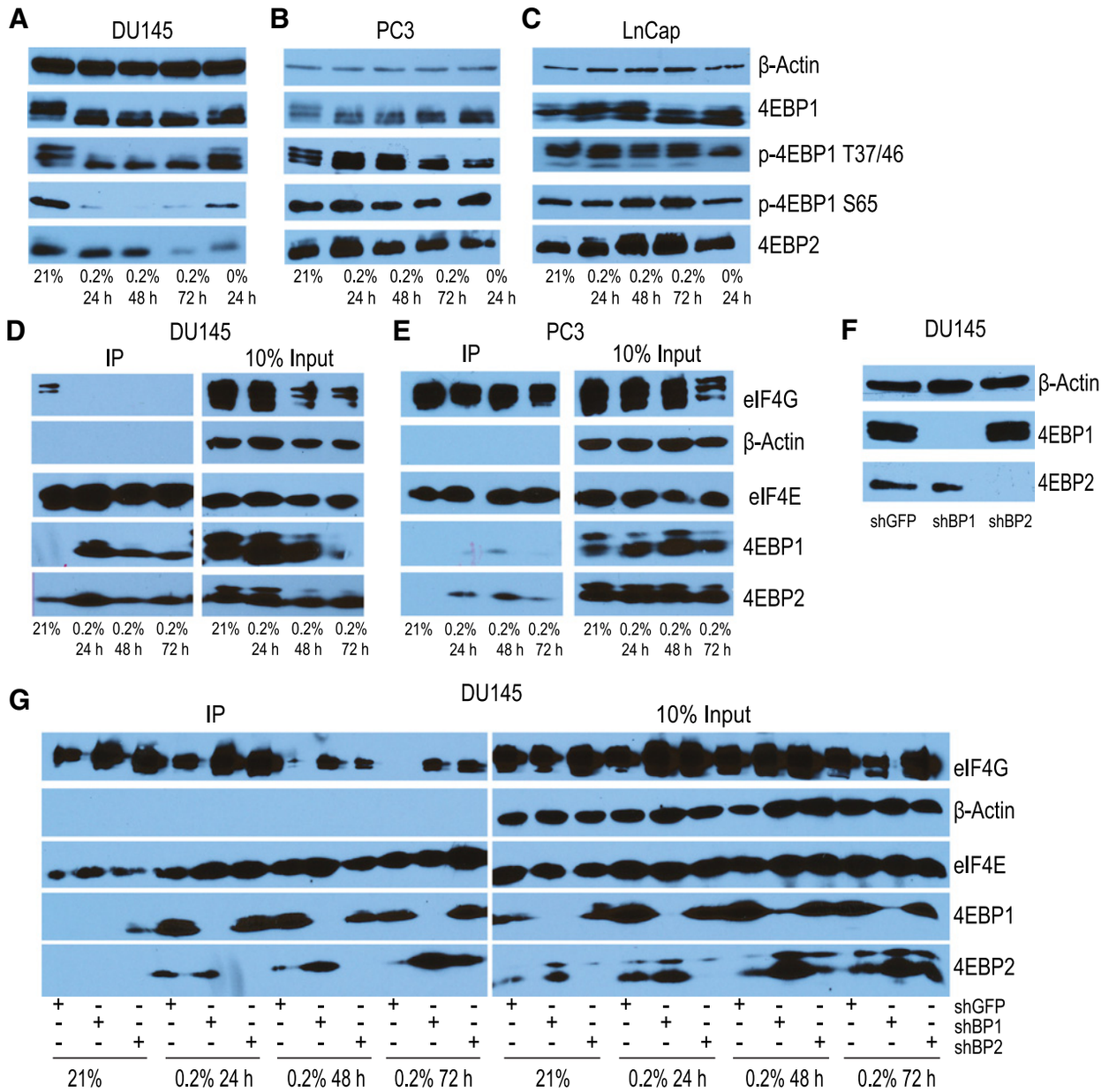

Figure 1.

mTOR downstream targets 4E-BP1 and 4E-BP2 are dephosphorylated during hypoxia and required to inhibit eIF4F formation during hypoxia in DU145 prostate cancer cells. DU145 (**A**), PC3 (**B**), and LNCAP (**C**) were exposed to the oxygen conditions indicated and analyzed by Western blotting using the antibodies indicated. DU145 cells (**D**) and PC3 cells (**E**) were exposed to the oxygen conditions as indicated, lysed, and the supernatant incubated with 7-methyl-GTP sepharose resin to pull down eIF4E. Immunoprecipitated proteins and 10% supernatant input were analyzed by Western blotting using the antibodies indicated. **F,** DU145 cells treated with lentivirus expressing three different shRNAs – shGFP, sh4E-BP1, sh4E-BP2 were analyzed by Western blotting using the antibodies indicated. **G,** DU145 cells expressing shGFP, sh4E-BP1 or sh4E-BP2 were exposed to the oxygen conditions as indicated, lysed, and the supernatant incubated with 7-methyl-GTP sepharose resin binding to pull down eIF4E. Immunoprecipitated proteins and 10% supernatant input were analyzed by Western blotting using the antibodies indicated.

using m7GTP Sepharose resin to pull down eIF4E protein were performed and assessed in a large gradient gel to detect the expression of eIF4G (200 kDa), eIF4E (25 kDa), and 4E-BP1 or 4E-BP2 (15–20 kDa) using Western blotting (Fig. 1D and E). During 21% normoxia conditions, eIF4E is associated with eIF4G, consistent with formation of an active eIF4F complex and efficient translation initiation (11). In DU145 cells, which had low levels of eIF4G bound to eIF4E, there was a dramatic decrease in the binding of eIF4G to eIF4E and a strong increase in the association of 4E-BP1 and 4E-BP2 with eIF4E during exposure to 0.2% O_2 at 24, 48, and 72 hours (Fig. 1D, lane 2–4) compared with 21% O_2 condition (Fig. 1D, lane 1). In PC3 cells (Fig. 1E), there was a large

amount of eIF4G binding to eIF4E during exposure to 21% O_2 and also at 0.2% O_2 for 24 to 72 hours, with only slightly increased levels of 4E-BP1 associated with eIF4E during 0.2% O_2 conditions. We also found a substantial increase in 4E-BP2 association with eIF4E during hypoxia. Thus, despite the increased binding of 4E-BP1and 4E-BP2 to eIF4E, there was only a modest effect on eIF4E association with eIF4G in PC3 cells, which was expressed at high levels in this cell line. Interestingly, we also observed a decrease in overall levels of eIF4G after longer times of hypoxia exposure (after 48 hours in DU145 and after 72 hours in PC3), which may exacerbate the effect of hypoxia on inhibition of the eIF4F complex. However, our data demonstrate that 4E-BP dephosphorylation during hypoxia strongly inhibits eIF4G binding to eIF4E within 24 hours in DU145 cells.

To understand the relative role of 4E-BP1 and 4E-BP2 in inhibiting eIF4F formation and mRNA cap-dependent translation initiation during hypoxia exposure in DU145 cells, we used lentivirus to infect and express two distinct shRNAs to knockdown 4E-BP1 or 4E-BP2 expression. DU145 cells expressing sh4E-BP1 or sh4E-BP2 resulted in efficient knockdown of 4E-BP1 or 4E-BP2 protein levels compared with a nontargeting shGFP control (Fig. 1F). We performed cap pulldown experiments on DU145 shGFP, sh4E-BP1, sh4E-BP2 cell lines during nomoxia and hypoxia conditions at different time points. eIF4G association with eIF4E decreased during exposure to 0.2% O_2 for 48 and 72 hours in DU145 shGFP control cells (Fig. 1G, lanes 7 and 10) compared with 21% O_2 and 0.2% O_2 24 hours (Fig. 1G, lanes 1 and 4). However, knockdown of either 4E-BP1 or 4E-BP2 was sufficient to restore eIF4G binding to eIF4E during exposure to 0.2% O_2 at 48 and 72 hours (Fig. 1G, lanes 8, 9, 11, and 12). These results demonstrate that both 4E-BP1 and 4E-BP2 contribute to decreased eIF4F formation and that depletion of both are required to prevent this formation in DU145 cells.

4E-BP1 and 4E-BP2 dephosphorylation during hypoxia is required to inhibit eIF4F formation in HCT116 colon cancer cells

To further examine the role of 4E-BP1 and 4E-BP2, we conducted similar experiments in HCT116 colon cancer cells, which have aberrant mTOR activation resulting from an activating mutation in PIK3CA (31). The levels of 4E-BP1, 4E-BP2, and phosphorylated 4E-BP1 (S65 and T37/46) were measured during hypoxia. Figure 2A demonstrates that like DU145 prostate cancer cells, 4E-BP1 was dephosphorylated after 24-hour exposure in 0.2% O_2 conditions, and maintained at 48 and 72 hours after 0.2% O_2 exposure. 4E-BP2 was noticeably dephosphorylated only at 72 hours in 0.2% O_2. Furthermore, there was no detectable S65 phosphorylation after 24-, 48-, and 72-hour exposure in 0.2% O_2. To assess the functional consequences of 4E-BP dephosphorylation during hypoxia, cap pulldowns were performed at different time points (Fig. 2B). As expected, there were no changes in eIF4E expression. A large amount of eIF4G association and low levels of 4E-BP1 were observed at 21% O_2 normoxia (Fig. 2B, lanes 1 and 2). In contrast, after 72-hour exposure to 0.2% hypoxia and 0% O_2 conditions, there was loss of eIF4G association and increases in both 4E-BP1 and 4E-BP2 (Fig. 2B, lanes 3 and 4). To further confirm the role of 4E-BP1 and 4E-BP2 individually, we knocked down each as described above for DU145 (Fig. 2C). During 21% O_2 conditions, there was no difference in eIF4G expression in 4E-BP1 knockdown, 4E-BP2 knockdown, and control shGFP cells. As seen earlier with DU145 cells, eIF4G association with eIF4E was partially restored during 72-hour exposure to 0.2% O_2 in each of the 4E-BP1 or 4E-BP2 knockdown cells (Fig. 2D, lanes 5 and 6) compared with a nontargeting control shGFP cell line (Fig. 2D, lane 4). Thus, in both DU145 prostate cancer and HCT116 colon cancer lines, both 4E-BP1 and 4E-BP2 contribute to inhibition of eIF4F and cap-dependent mRNA translation during hypoxia.

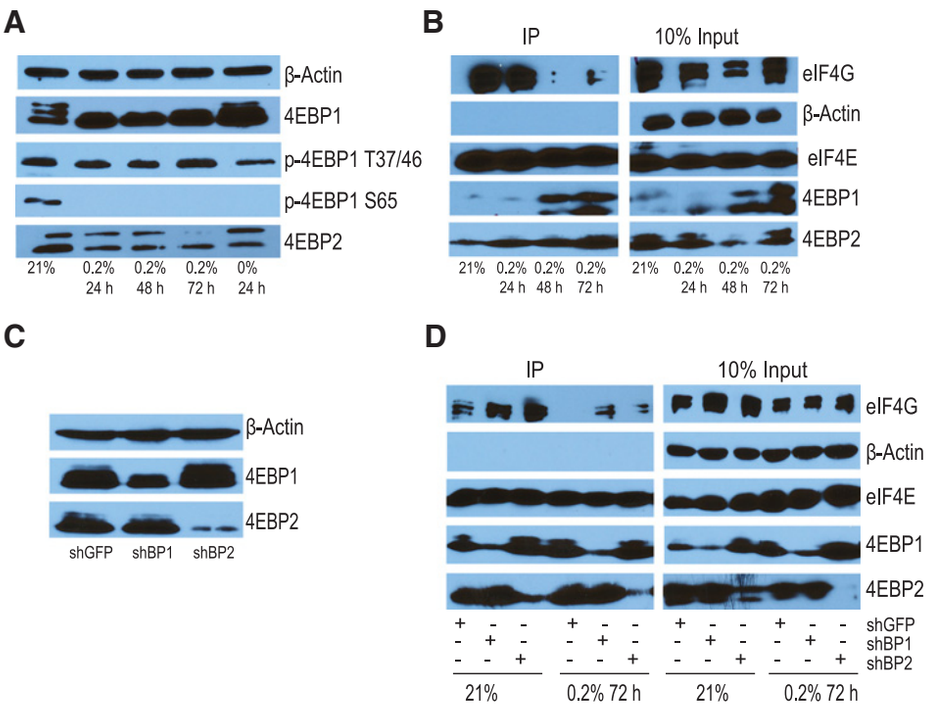

Figure 2.
4E-BP1 and 4E-BP2 are dephosphorylated during hypoxia and are required to inhibit eIF4F formation in HCT116 colon cancer cells. **A,** HCT116 cells were exposed were exposed to the oxygen conditions indicated and analyzed by Western blotting using the antibodies indicated. **B,** HCT116 cells were exposed to the oxygen conditions as indicated, lysed, and the supernatant incubated with 7-methyl-GTP sepharose resin to pull down eIF4E. Immunoprecipitated proteins and 10% supernatant input were analyzed by Western blotting using the antibodies indicated. **C,** HCT116 cells treated with lentivirus expressing three different shRNAs – shGFP, sh4E-BP1, sh4E-BP2 were analyzed by Western blotting using the antibodies indicated. **D,** HCT116 cells expressing shGFP, sh4E-BP1, or sh4E-BP2 were exposed to the oxygen conditions as indicated, lysed, and the supernatant incubated with 7-methyl-GTP sepharose resin binding to pull down eIF4E. Immunoprecipitated proteins and 10% supernatant input were analyzed by Western blotting using the antibodies indicated.

4E-BP1 or 4E-BP2 knockdown reduces hypoxia tolerance in HCT116 and DU145 cells

To determine the phenotypic properties of 4E-BP1 and 4E-BP2 on tumor hypoxia tolerance, we created stable knockdown of 4E-BP1 and 4E-BP2 using lentiviruses expressing shRNAs against both of these individually or in combination (Fig. 3A) and assessed the overall toxicity of hypoxia exposure of differing periods using the clonogenic assay. In Fig. 3B, DU145 prostate cancer cells with knockdown of either 4E-BP1 or 4E-BP2 knockdown demonstrated substantial reduced surviving fractions in 0.2% hypoxia at all time points evaluated. The reduction in hypoxia tolerance was more severe following knockdown of 4E-BP1 than with knockdown of 4E-BP2 knockdown, perhaps due to higher expression of 4E-BP1. However, the data clearly

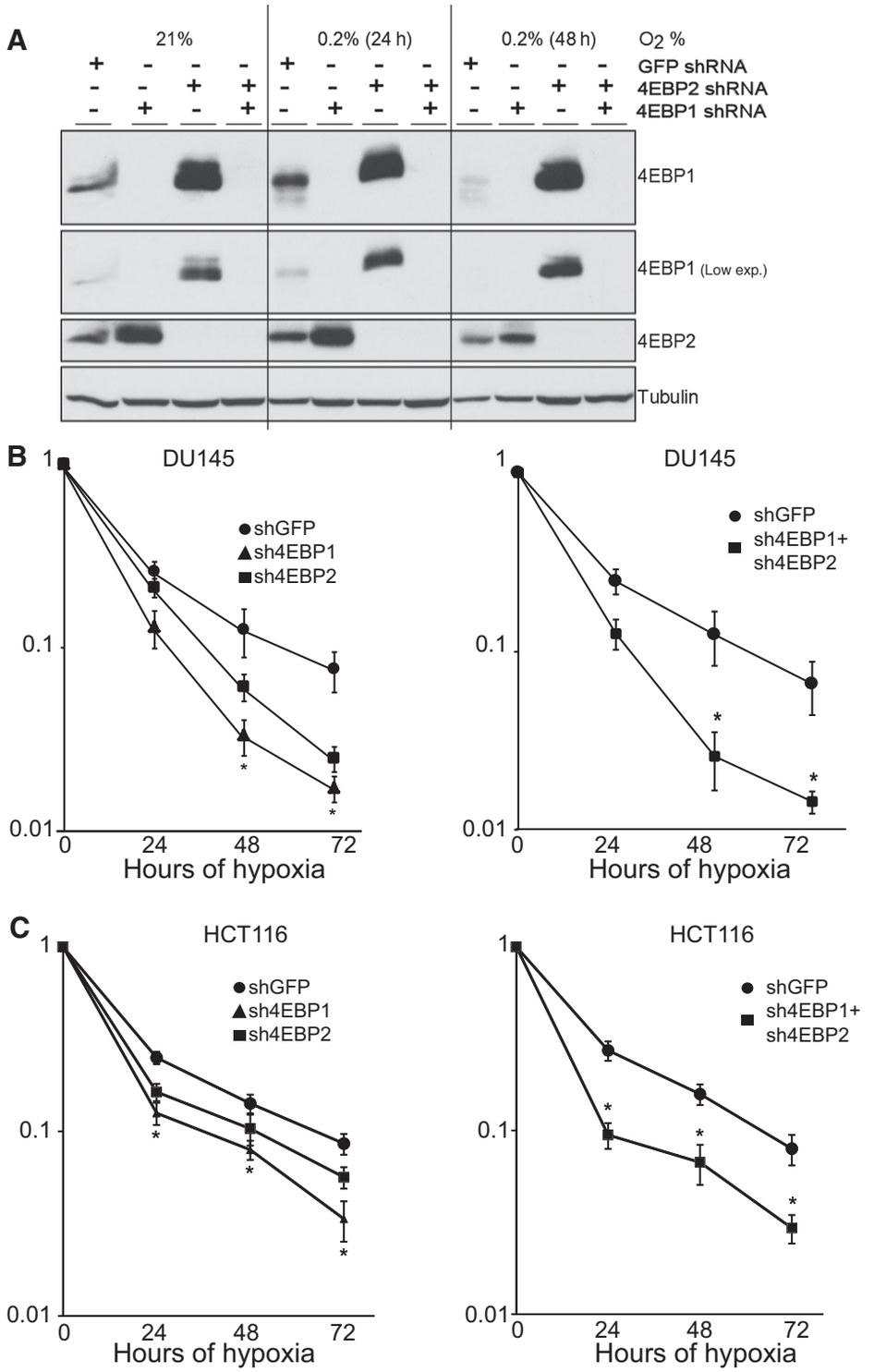

Figure 3.

4E-BP1 or 4E-BP2 knockdown reduces hypoxia tolerance. **A,** Western blot analysis for 4E-BP1, 4E-BP2, and γ-tubulin in DU145 cells following knockdown with the indicated shRNA lentiviruses. **B** and **C,** Clonogenic assays evaluating the toxicity of hypoxia (0.2% O_2) for the indicated periods of time for DU145 prostate cancer (**B**) and HCT116 colon cancer (**C**) cells following knockdown with the indicated lentiviruses.

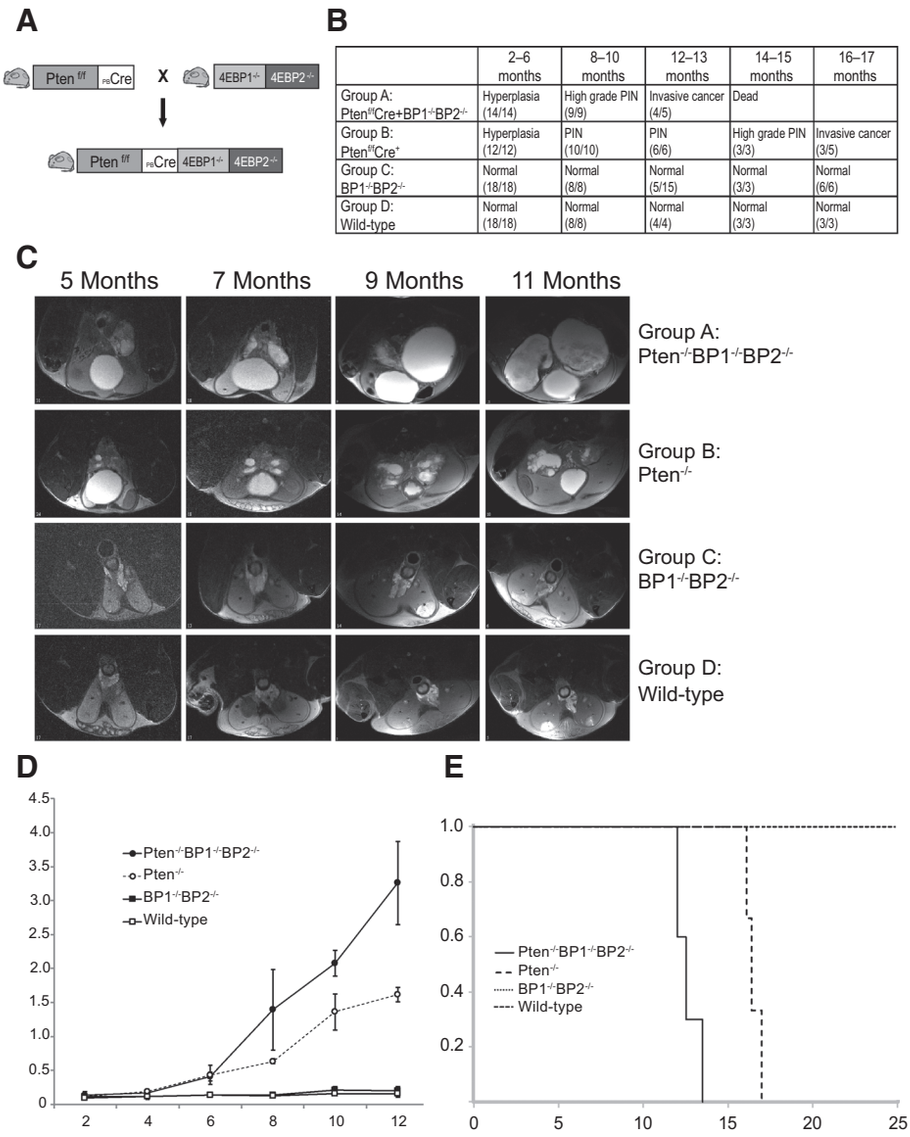

	2–6 months	8–10 months	12–13 months	14–15 months	16–17 months
Group A: Pten$^{f/f}$Cre+BP1$^{-/-}$BP2$^{-/-}$	Hyperplasia (14/14)	High grade PIN (9/9)	Invasive cancer (4/5)	Dead	
Group B: Pten$^{f/f}$Cre^{+}	Hyperplasia (12/12)	PIN (10/10)	PIN (6/6)	High grade PIN (3/3)	Invasive cancer (3/5)
Group C: BP1$^{-/-}$BP2$^{-/-}$	Normal (18/18)	Normal (8/8)	Normal (5/15)	Normal (3/3)	Normal (6/6)
Group D: Wild-type	Normal (18/18)	Normal (8/8)	Normal (4/4)	Normal (3/3)	Normal (3/3)

Figure 4.
Loss of 4E-BP1 and 4E-BP2 increase tumorigenesis in a prostate cancer mouse model. **A,** Breeding strategy and analysis of cancer development in four genotypes. Pten$^{flox/flox}$/Probasin-Cre mice were bred to mice with 4E-BP1/2 double knockout mice: Cre-mediated excision leads to loss of Pten gene in prostate epithelium in 4E-BP1/2 knockout background. **B,** Four groups of mice were separated according to genotyping results as indicated. Cohorts of each group of mice were analyzed at 2–6 months, 8–10 months, 12–13 months, 14–15 months, 16–17 months. All mice in Group A died before 14 months of age. The number of mice in each group analyzed at different time points are indicated in brackets. **C,** MRI imaging: representative T2-weighted images of the murine prostate gland and surrounding region, from each cohort and time-point, demonstrating group differences in enlargement of the prostate gland volume over time. **D,** The weight of prostates in each group at different time points was measured. **E,** Kaplan–Meier survival curve shows that mice in Group B with Pten KO survive approximately 4 months longer than mice in Group A with Pten KO + 4E-BP1/2 KO background. Survival curves were compared using the log-rank test.

demonstrate a role for both proteins in promoting hypoxia tolerance. Correspondingly, dual knockdown both 4E-BP1 and 4E-BP2 led to a somewhat further decrease in hypoxia tolerance. Similar to that observed in DU145 cells, 4EBP1 and/or 4E-BP2 knockdown reduced clonogenic survival following exposure to 0.2% O_2 in HCT116 colon cancer cells (Fig. 3C). In this line, the survival of 4E-BP1 knockdown lines was also lower than 4E-BP2 knockdown. These data indicate that in both of the mTOR-deregulated cell lines examined, 4E-BP1 and 4E-BP2 are able to be dephosphorylated during hypoxia, and are required to prevent eIF4F formation and to preserve hypoxia tolerance during hypoxia.

Loss of 4E-BP1 and 4E-BP2 gene function in a prostate cancer mouse model with Pten deficiency increases tumorigenesis

To investigate the functional role of 4E-BP1 and 4E-BP2 in prostate cancer development and tumor hypoxia *in vivo*, we crossed 4E-BP1 and 4E-BP2 knockout mice into a well-established prostate cancer mouse model driven by conditional Pten gene deletion. In this model, Pten is specifically lost in prostate epithelial cells by crossing mice with homozygous floxed Pten alleles (Pten$^{flox/flox}$) to the prostate epithelial promoter - Probasin-mediated Cre mice (Probasin-Cre). The Pten$^{flox/flox}$/Probasin-Cre transgenic mice have been shown to develop invasive adenocarcinoma at 16–17 months of age (25). By crossing the Pten$^{flox/flox}$/Probasin-Cre to a mouse line with 4E-BP1 and 4E-BP2 gene double knockouts in ref. 26, we created 4E-BP1 and 4E-BP2 gene double knockouts in this prostate cancer mouse model (Pten$^{flox/flox}$/Probasin-Cre/4E-BP1/2 KO; Fig. 4A). Mice with deletion of Pten and/or 4E-BP1/4E-BP2 gene were confirmed by PCR (Supplementary Fig. S1A–S1D). We separated mice offspring into four groups according to different genotyping results: Group A: 4E-BP1/2 KO + Pten KO, Group B: Pten KO only, Group C: 4E-BP1/2 KO, Group D: wild-type (Fig. 4A). Group C and Group D were considered as control groups. The frequencies among different groups follow Mendelian ratios.

To assess phenotypes among different groups of mice, especially between Group A and Group B, cohorts of each were

analyzed at 2–6 months (Group A $n = 14$, Group B $n = 12$, Group C $n = 18$, Group D $n = 19$), 8–10 months (Group A $n = 9$, Group B $n = 10$, Group C $n = 8$, Group D $n = 8$), 12–13 months (Group A $n = 5$, Group B $n = 6$, Group C $n = 5$, Group D $n = 4$), 14–15 months (Group B $n = 3$, Group C $n = 3$, Group D $n = 3$), and 16–17 months of age (Group B $n = 5$, Group C $n = 6$, Group D $n = 3$; Fig. 4A). We found that all cohorts of mice in Group A developed aggressive disease and died before 14 months of age; however, mice in Group B survived until 17–18 months of age. Mice in Group C and Group D have the same life span as normal mice (Fig. 4A).

We monitored prostate cancer development and other morphologic changes over time using MRI. We observed morphologic changes in the prostate gland in these four groups of mice between 5 months and 12 months of age (Fig. 4B). Obvious differences in glandular shapes and volumes were observed in Group A compared with Group B after 6–7 months, presenting as balloon-like structures of high T2-weighted MRI signal intensity which were noted as filled with secretory fluids and enlarged glandular components upon dissection (data not shown). After 11–12 months of age, the prostate glands of mice in Group A were very large compared with other groups of mice.

Second, cohorts of mice in these four different groups were sacrificed at different times ranging from 2 months to17 months of age bimonthly. The weight of the prostates was measured after dissection (Fig. 4C). After 6 months of age, the weight of the mice prostate in Group A increase significantly over the other groups; and the mice prostate in Group B also increase, but much less than mice in Group A (Fig. 4C). Histologic and pathologic analysis showed that during 2–6 months of age, 14 of 14 mice in Group A with Pten KO + 4E-BP1/2 KO and 12 of 12 mice in Group B with Pten KO only develop glandular hyperplasia in the prostate compared with normal control Groups C and D (Supplementary Fig. S2A). Around 8–10 months of age (Fig. 5A; Supplementary Fig. S2B), 9 of 9 mice in Group A demonstrated massive hyperplasia within the prostatic gland with nuclear features consistent with PIN to high-grade PIN (prostate intraepithelial neoplasia). Compared with Group A, 10 of 10 mice in Group B demonstrated a much more moderate level of glandular hyperplasia and similarly more moderate nuclear features. At 12–13 months of age (Fig. 5B), 4 of 5 mice in Group A demonstrated intense glandular hyperplasia invading stroma, features consistent with invasive prostate adenocarcinoma. However, 6 of 6 mice in Group B at the same time showed only contained intraglandular hyperplasia and nuclear features consistent with PIN. Mice in Group A did not survive longer than 14 months of age. In contrast, mice in Group B progressed towards adenocarcinoma at a much slower rate (Fig. 4E). At 14 months of age, 3 of 3 mice in Group B showed initial features of more intense prostate glandular proliferation and nuclear atypia consistent with PIN (Supplementary Fig. S2C). Around 16–17 months of age (Fig. 5C), 3 of 5 mice in Group B were found to have developed an invasive phenotype consistent with adenocarcinoma, which is similar to that reported for this model by other research groups (25). Mice in control Group C with 4E-BP1/2 KO from 10 months of age to 17 months of age were found to have minor abnormal features including slightly enlarged nuclei and occasionally with one or a few conspicuous nucleoli as compared with the wild-type prostate glands in Group D. These results suggest that loss of 4E-BP1/2 gene function in Pten-deficient mouse model accelerates prostate tumorigenesis.

Immunostaining tests for 4E-BP1 and 4E-BP2 confirmed the deletion of 4E-BP1 and 4E-BP2 protein in the mice of Group A (Fig. 5D and E). Similarly, a phosphorylation-specific AKT antibody confirmed AKT activation in Group A and B only with high immunostaining signals around the plasma membrane as expected.

Loss of 4E-BP1 and 4E-BP2 gene function in Pten-deficient prostate mouse model increases vascular density and reduces hypoxia tolerance

Previous results have demonstrated that importance of eIF4E phosphorylation in driving tumorigenesis in a similar prostate cancer mouse model (32). We therefore evaluated if eIF4E phosphorylation differed in mice with Pten deficiency versus those with both Pten and 4E-BP1 and 4E-BP2 deficiency. Immunostaining for eIF4E phosphorylation in Group A and Group B at 10 and at 12 months of age showed substantially increased phosphorylation in the prostate epithelium relative to wild-type mice, but no differences between those with or without the 4E-BPs (Supplementary Fig. S3). Consequently, eIF4E phosphorylation cannot account for the differences between cancer development in these groups. eIF4E activation has also been shown to drive proliferation and we hypothesized that the differences in cancer development between Groups A and B may be due to differential proliferation. However, there was no significant difference in Ki67 immunostaining between mice of Groups A and B measured at 8 or 12 months and also no correlation between proliferation and stage of prostate cancer development (Fig. 6A and B). These data indicate that loss of Pten is sufficient to drive the prostate epithelial cells into a constitutive proliferative mode, and that this is not further augmented by 4E-BP1 and 4E-BP2 loss or other events in prostate cancer progression.

We also probed differences in vascularity of the prostate lesions over time at 8, 12, and 16 months. At 8 and 12 months, significantly higher CD31 immunostaining signals were observed in mice of Group A, demonstrating that increased vascular density in Group A compared with Group B (Fig. 6C and D) at equivalent points of time. This acceleration of vascularity was consistent with the more rapid progression of the Pten-deficient 4E-BP1 and 4E-BP2 knockout mice. Vascularity also increased to similar levels in the 4E-BP proficient mice, but at later time points where prostate lesions progressed. However, even at 16 months, the overall vascularity in the 4E-BP1 and 4E-BP2–proficient tumors was reduced compared with the knockout tumors suggesting that this pathway may play a key role in driving angiogenesis.

Finally, given the important role of mTOR suppression and 4E-BP phosphorylation in suppressing protein synthesis during hypoxia, we also assessed differences in hypoxia and hypoxia tolerance in these models. We hypothesized that in the presence of aberrant mTOR, 4E-BP1, and 4E-BP2 would still be required during hypoxia to suppress eIF4F formation and promote hypoxia tolerance. To test this hypothesis, we measured viable areas of tumor hypoxia using hypoxia marker EF5 in mice from Groups A and B at 10, 12, and 16 months of age. We found that EF5 staining of viable hypoxic cells was very strong in mice of Group A at 10 months when they had developed high-grade PIN, but was reduced significantly at 12 months when invasive cancer had been established (Fig. 6E). The quantification of EF5 immunostaining also showed that the differences between 10 months and 12 months old of mice in Group A were significant (Fig. 6F). In contrast, in mice of Group B, there was less red EF5 immunostaining signals at 10 months and 12 months (low-grade PIN stage) consistent with the slow progression in this model, but that

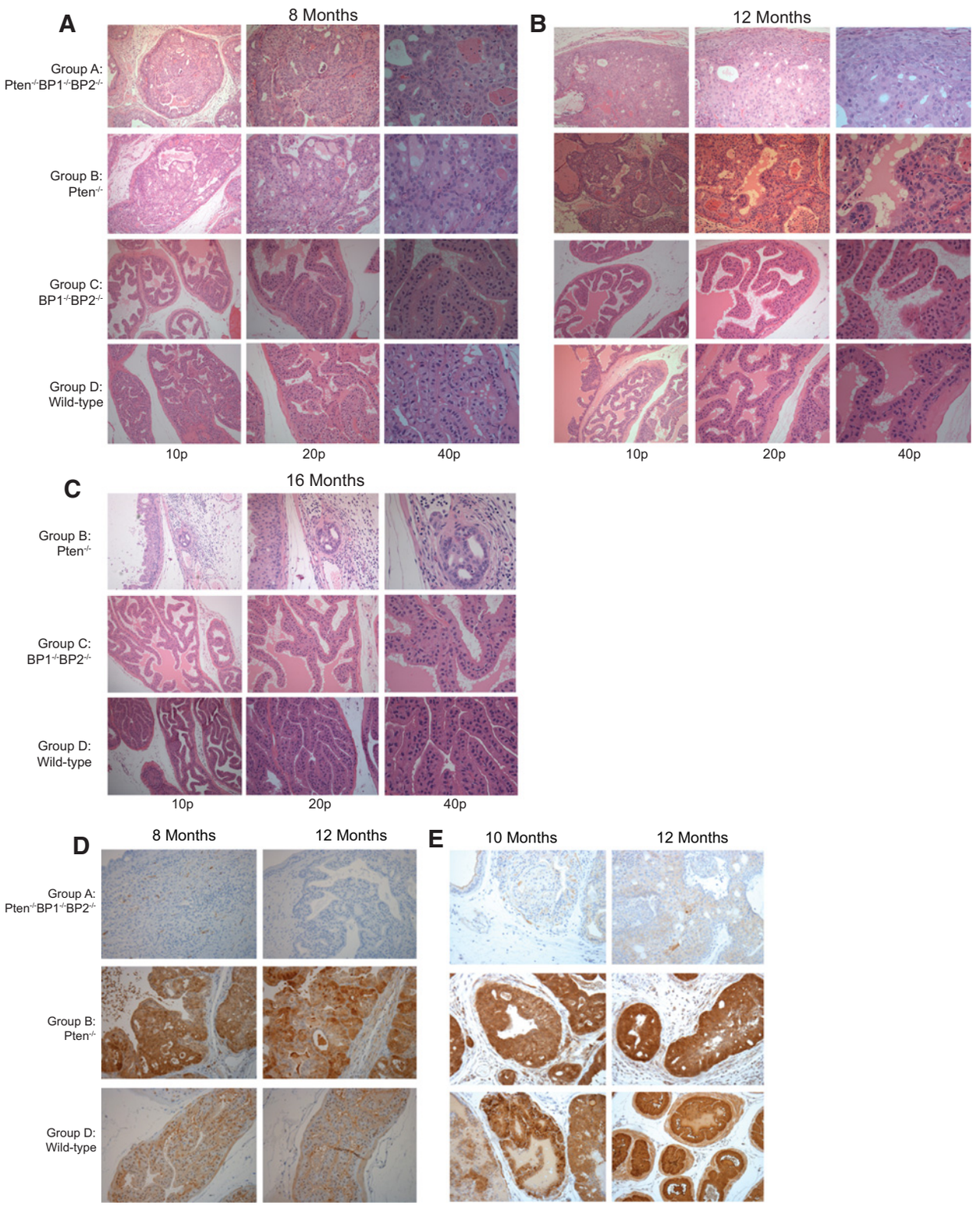

hypoxia increased substantially at the time when these mice had developed invasive cancer at 16 months of age (Fig. E and F). These data imply that at the stages where prostate cancer had developed (10 months: for Group A and 16 months for Group B), the tumors lacking 4E-BP1 and 4E-BP2 have significantly less hypoxia. Although it is difficult to set a threshold on where true malignancy occurs in each model, these data indicate that as malignancy evolves in the tumors lacking 4E-BP1 and 4E-BP2 they show decreased levels of hypoxia, consistent with an inability to support hypoxic cell survival. The 4E-BP wild-type mice show the opposite with increased levels of hypoxia in the mature tumors.

To understand whether the decreasing hypoxia observed during tumor development in mice of Group A was due to loss of hypoxia tolerance, we performed the EF5/Caspase-3 double immunostaining on tumor samples. The results demonstrate significantly higher caspase-3 signals within hypoxia regions (green + red) region in Group A 4E-BP1 and 4E-BP2 knockout mice compared with Group B at 10 months and at 12 months of age (Fig. 6G and H). At 12 months of age, caspase-3 activation was significantly reduced in hypoxia regions in mice of Group A. In mice of Group B, there were several weak caspase-3 signals in hypoxia at 10 months and 12 months of age (Fig. 6G and H). The caspase-3 signals became stronger in red EF5 hypoxia region in mice of Group B at 16 months of age, when the prostate cancer has been fully developed. These data show that hypoxic cells do not survive in mice of Group A during tumor development, and that expression of 4E-BP1 and 4E-BP2 in the presence of Pten deficiency may be critical for cancer cells to survive hypoxia in the presence of aberrant mTOR activation.

Discussion

Our study reveals two key aspects on the role of the mTOR targets 4E-BP1 and 4E-BP2 in the development and aggressiveness of prostate cancer. First, we found that loss of these negative regulators of mTOR signaling accelerated prostate cancer development in a mouse model driven by PTEN deficiency in the prostate. Thus, even in the case of deregulated PI3K signaling and constitutive mTOR activation, 4E-BP1 and 4E-BP2 constrained signaling downstream of mTOR. Interestingly, this effect appears to be unrelated to effects on cell proliferation. We found no difference in eIF4E phosphorylation, PI3K activation, or proliferation as assessed by Ki67 or EdU incorporation (data not shown) between prostate cancer mice with knockout of 4E-BP1/2 and wild-type. However, we did find that accelerated tumorigenesis was associated with a significant increase in angiogenesis and vascular development as assessed by increased in CD31 immunostaining. These results are similar to observations reported in a carcinogen-induced lung cancer model in 4E-BP1/2 KO mice (33). These mice also showed accelerated tumorigenesis (albeit in the absence of a defined upstream activator of mTOR) without significant changes in proliferation between the WT 4E-BP1/2 KO mice. In addition, the lung cancers arising in the 4E-BP1/2 KO mice demonstrated elevated microvessel density by CD31 immunostaining.

Second, our study demonstrates that although loss of 4E-BP1 and 4E-BP2 accelerates prostate cancer development, the tumors that do develop have reduced levels of hypoxic cells. Hypoxic levels dropped substantially during the development of PTEN loss–driven prostate cancer in the 4E-BP1/2 KO mice, whereas they increased as cancer developed in the WT mice. Hypoxia is a known negative prognostic indicator in prostate cancer, associated with treatment resistance, increased metastasis, and increased genomic instability. Consequently, although these tumors develop more rapidly, they are associated with a subtype of prostate cancer that in humans has a better prognosis due to less hypoxia.

Increased microvessel density in the 4E-BP1/2 KO tumors may contribute to the reduced levels of hypoxia in these tumors, although high CD31 levels were observed throughout progression from PIN to cancer, whereas hypoxic levels dropped only once cancers had developed. Our data indicate that 4E-BP1/2 are important during hypoxia to promote cell survival in cells with aberrant mTOR activation. Hypoxia suppresses mTOR signaling to inhibit translation and conserve energy, and *in vitro* we found that loss of 4E-BP1 and 4E-BP2 compromised the ability of hypoxic cells to survive hypoxic stress. We examined changes in

Figure 5.

Histologic examination of prostates from mouse cohorts. Selective deletion of Pten in the prostate gland epithelium in 4E-BP1/2 knockout accelerates tumorigenesis. **A,** Comparsion of prostate tumorigenesis at 8 months of age: In Group A (row 1), prostatic glands were distended by proliferation of glandular cells (10p). At intermediate magnification (20p), the glands filling up the lumen have a disordered architecture with back to back acini while lacking intervening stroma. At high power (40p), the nuclei show moderate nuclear enlargement and conspicuous nucleoli. In Group B (row 2), antecedent prostatic gland distended by proliferation of glandular cells with little lumen left (10p). At intermediate magnification (20p) the glands filling up the lumen display a cribriform architecture lacking intervening stroma. At high power (40p), the nuclei show moderate nuclear enlargement and conspicuous nucleoli. In Groups C and D (row 3 and 4), normal sized prostatic glands, showing infoldings of the lining epithelial cells (10p). The one-layered lining epithelial cells projecting into the lumen are supported by a thin layer of fibrovascular stroma (20p). At high magnification (40p), the nuclei are small and dense and nucleoli are inconspicuous. **B,** Comparision of prostate tumorigenesis at 12 months of age: In Group A (row 1), at low power (10p), a large well-demarcated mass of glandular cells is seen, containing variable-sized acini. At intermediate power (20p), the arrangement of the glandular cells in densely packed acini and strands without intervening stroma can be appreciated. At high power (40p), cytonuclear atypia is prominent, accompanied by mitotic activity. In Group B (row 2), antecedent prostatic glands distended by proliferation of glandular cells with little lumen left (10p). At intermediate magnification, the glands filling up the lumen display a cribriform architecture lacking intervening stroma (20p). At high power (40p), the nuclei show moderate nuclear enlargement and conspicuous nucleoli. In Group C, occasional slightly enlarged nuclei are noted (row 3). In Group D (row 4), the prostate glands are morphologically normal. **C,** At 16 months of age, no mice in Group A remained as they did not survive more than 14 months old. In Group B (row 1), at the left a distended gland, lined by epithelial cells and in the centre a few glands in the stroma (10p). At intermediate magnification (20p), the distended gland at the left appears to be lined by multilayered glandular epithelium showing some cytonuclear atypia. The small focus of glands in the stroma is in the vicinity of a blood vessel with a small tumor nest protruding in the vascular lumen (vascular invasion by carcinoma) as highlighted at higher magnification (40p). In Group C (row 2), at lower power, prostate glands are normal-sized with infoldings of the glandular lining (10p), supported by a thin layer of stroma (20p), with nuclei slightly enlarged and occasionally with one or a few conspicuous nucleoli (40p) as compared with the wild-type prostate glands of the same age at high power. In Group D (row 3), normal prostate gland. **D,** Immunostaining demonstrates that the 4E-BP1 gene was knocked out in Group A compared with Groups B and D at 8 months and 12 months of age. Original magnification, 10p. **E,** Immunostaining demonstrated that 4E-BP2 gene was knocked out in Group A compared with Groups B and D at 10 months and 12 months of age. Original magnification, 10p.

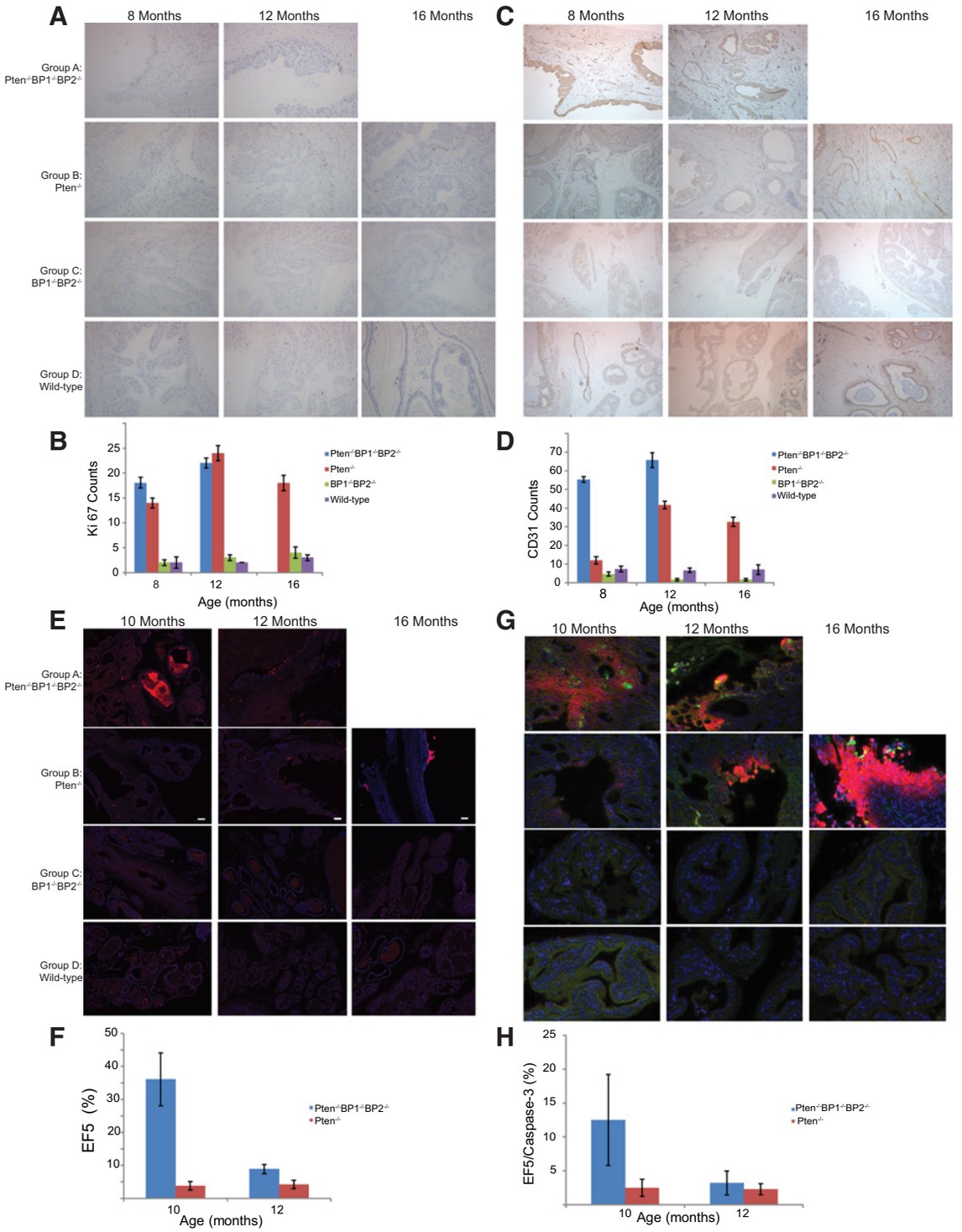

Figure 6.

Loss of 4E-BP1/2 gene expressions in prostate cancer model with Pten gene deficiency leads to increased vascular density and reduce hypoxia tolerance. **A,** Ki 67 immunostaining demonstrated that increased proliferative activity of prostate epithelial cells both in Groups A and B compared with control Groups C and D at 8 months, 12 months, and 16 months of age. Original magnification, 2,000×. **B,** Ki 67 immunostaining quantification. No significant difference between mice in Groups A and B, but Ki-67 labeling was higher in both Groups A and B than control Groups C and D at 8 months, 12 months, and 16 months of age. **C,** CD31 immumostaining demonstrated increased vascular density in Group A compared with Group B and control group at 8 months, 12 months, and 16 months of age. Original magnification, 1,000×. (*Continued on the following page.*)

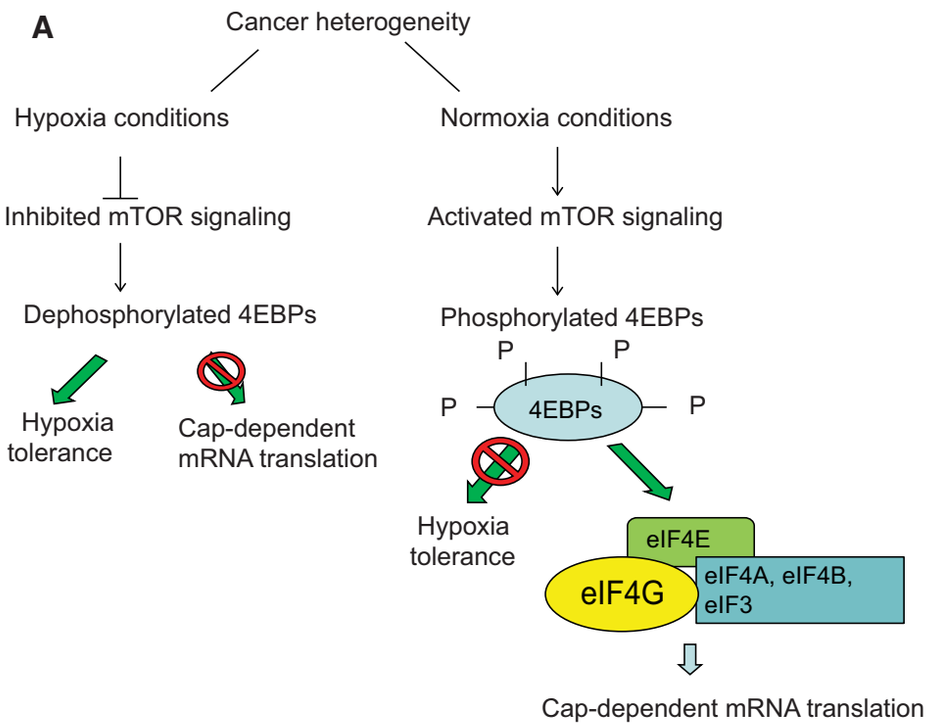

Figure 7.
Principle of mTOR signaling in tumor normoxia and hypoxia. In cancer heterogeneity, the function of mTOR signaling is different between tumor normoxia and hypoxia. In normoxia conditions, mTOR signaling is activated, and phosphorylated downstream factors 4E-BPs release eIF4E, which combine eIF4G and other factors such as eIF4A and eIF4B to initiate mRNA cap-dependent translation. In contrast, in hypoxia conditions, mTOR signaling is inhibited and dephosphorylated 4E-BPs binds to eIF4E, which cannot combine eIF4G to initiate mRNA cap-dependent translation.

4E-BP1/2 phosphorylation and function during hypoxia in PC3, LNCAP, and DU145 prostate cancer cell lines. In the DU145 cell line, we showed that 4E-BPs were dephosphorylated rapidly during mild hypoxia (0.2% O_2), inhibited eIF4E binding to eIF4G, and were required to promote cell survival. Milder effects were observed on 4E-BP phosphorylation in PC3 cells but with similar kinetics, whereas LNCAP cells showed no changes in phosphorylation until 72 hours of 0.2% O_2. Interestingly, DU145 and PC3 cells have a reported loss-of-function mutation in PTEN, whereas LNCAP does not (Cancer Cell Line Encyclopedia). However, we observed a similar effect on 4E-BP phosphorylation and requirement for 4E-BP to promote hypoxia tolerance in the colon cancer cell line HCT116, which harbors a PIK3CA mutation and consequently elevated mTOR signaling. Thus, our data suggest that PTEN loss–driven cancers need to maintain some ability to suppress signaling downstream of mTOR to promote survival during times of oxygen limitation.

In this study, our data indicate that both 4E-BP1 and 4E-BP2 are involved and important factors in preventing eIF4F formation and cap-dependent mRNA translation during hypoxia. This suggests that 4E-BP1 and 4E-BP2 have similar and partially redundant functions in regulating eIF4E during hypoxia. Although both 4E-BP1 and 4E-BP2 knockdown can reduce hypoxia tolerance in HCT116 and DU145 cell lines, 4E-BP1 appeared to provide a higher level of tolerance to hypoxia. The 4E-BP family has three proteins in mammals—4E-BP1, 4E-BP2, and 4E-BP3. Although 4E-BP1 and 4E-BP2 have been shown to be regulated in a similar manner, the role of 4E-BP2 is reported to be weaker than that of 4E-BP1 in response to ischemia/reperfusion stress (13) and insulin treatment (14), which may be related to the relative expression of these two different proteins. Consistent with our findings, 4E-BP1 is also reported as the major factor regulating cap-dependent translation by AKT and MEK signaling in HCT116 cells (34). 4E-BP3 shares the basic structural and functional features of 4E-BP1 and 4E-BP2, but its regulation is unique and different (35). Phosphorylation sites that are critical for regulation of 4E-BP1 and 4E-BP2 by mTOR (36) are absent from 4E-BP3. 4E-BP3 has been reported to bind to nuclear eIF4E and inhibit eIF4E-mediated mRNA export (37). Our studies do not address a

(*Continued*.) **D,** CD31 immunostaining quantification: significantly higher CD31 immunostaining counting signals in Group A than Group B at 8 and 12 months of age. Both Groups A and/or B are significantly different from control Groups C and D at 8 months, 12 months, and 16 months of age (*, $P < 0.05$). **E,** Images with EF5 staining (red) and DAPI counterstain (blue) were obtained from immunofluorescence-stained slides digitized at 1 μm/pixel resolution on a Huron Technologies TissueScope scanner. Scale bar shows 200 mm width. In Group A, there are very strong EF5 signal at 10 months and less EF5 signal at 12 months old. In contrast, in Group B, there are less EF5 signal at 10 months and 12 months; but there is a stronger EF5 signal in 16 months of age. **F,** Image analysis was quantified using Definiens TissueStudio software. There are significantly higher EF staining cells at 10 months than at 12 months in Group A with 4E-BPs KO&Pten KO (*, $P < 0.05$). There are significantly higher EF5 staining cells at 16 months than that in 10 months and 12 months in Group B with Pten KO only (*$P < 0.05$). **G,** EF5/Caspase-3 double coexpression cells in mice of Group A is significantly more frequent than in mice of Group B at 10 months of age (*, $P < 0.05$). Images with EF5 staining (red) and caspase 3 (green) were obtained from immunofluorescence stained slides digitized at 1 μm/pixel resolution on a Huron Technologies TissueScope scanner. Scale bar shows 50 mm width. **H,** There are higher caspase-3 and EF5 overlapping signals in mice of Group A at 10 months, and there are less overlapping signals in mice of Group A at 12 months old. There is much less caspase-3 and EF5 overlapping signals in mice of Group B at both 10 and 12 months old. Green caspase signals at the edge of red EF5 signal region were demonstrated in mice of Group B at 16 months of age. There were no red or green signals on mice in control Groups C and D at 10 and 12 months of age.

potential residual function for 4E-BP3 in suppressing translation and contributing to hypoxia tolerance.

In summary, in this study we have demonstrated key roles for 4E-BP1 and 4E-BP2 during tumor development and during tumor hypoxia. We find that these factors maintain an ability to slow tumor progression in prostate cancer in the face of constitutive mTOR activation arising from loss of PTEN, and are also important in promoting survival of hypoxic cells once cancer has developed (Fig. 7). These findings have implications for use of mTOR inhibitors alone or in combination in cancer which function in a manner analogous to loss of 4E-BP1/2. Although such inhibitors may slow proliferation associated with activated mTOR gene regulation, they may also promote the survival of hypoxic cells that are resistant to other forms of therapy. Conversely, our *in vitro* data and new mouse model suggest that targeting 4E-BPs may be a novel way to selectively target and kill hypoxic cells in PTEN-deficient or mTOR-activated tumors.

Disclosure of Potential Conflicts of Interest

No potential conflicts of interest were disclosed.

Authors' Contributions

Conception and design: M. Koritzinsky, B.G. Wouters
Development of methodology: M. Ding, R. Vellanki, W. Foltz, T. McKee, B.G. Wouters
Acquisition of data (provided animals, acquired and managed patients, provided facilities, etc.): M. Ding, T. van der Kwast, W. Foltz, T. McKee, P.P. Pandolfi
Analysis and interpretation of data (e.g., statistical analysis, biostatistics, computational analysis): M. Ding, T. van der Kwast, R. Vellanki, T. McKee, B.G. Wouters
Writing, review, and/or revision of the manuscript: M. Ding, T. van der Kwast, R. Vellanki, W. Foltz, T. McKee, B.G. Wouters
Administrative, technical, or material support (i.e., reporting or organizing data, constructing databases): M. Ding, N. Sonenberg, B.G. Wouters
Study supervision: M. Ding, M. Koritzinsky, B.G. Wouters

Acknowledgments

This research was supported by grants from the Ontario Ministry of Health and Long Term Care (OMOHLTC), the Terry Fox Research Institute (TFRI-PPG 1036), the Ontario Institute for Cancer Research, the Canadian Institute for Health Research (CIHR grant 201592; to B. Wouters). M. Ding was supported by an EIRR21 postdoctoral fellowship from Department of Radiation Oncology, University of Toronto.

The authors would like to thank Jenna Sykes, Melania Pintilie for assisting with the statistical analysis. We thank Trevor Do, Junyan Zhang, and May S.M. Cheung for their technical assistance.

The costs of publication of this article were defrayed in part by the payment of page charges. This article must therefore be hereby marked *advertisement* in accordance with 18 U.S.C. Section 1734 solely to indicate this fact.

Received November 26, 2017; revised January 11, 2018; accepted January 23, 2018; published first February 16, 2018.

References

1. Brown JM, Wilson WR. Exploiting tumour hypoxia in cancer treatment. Nat Rev Cancer 2004;4:437–47.
2. Dal Pra A, Locke JA, Borst G, Supiot S, Bristow RG. Mechanistic insights into molecular targeting and combined modality therapy for aggressive, localized prostate cancer. Front Oncol 2016;6:24.
3. Wouters BG, Koritzinsky M. Hypoxia signalling through mTOR and the unfolded protein response in cancer. Nat Rev Cancer 2008;8:851–64.
4. Harris AL. Hypoxia–a key regulatory factor in tumour growth. Nat Rev Cancer 2002;2:38–47.
5. Koritzinsky M, Magagnin MG, van den Beucken T, Seigneuric R, Savelkouls K, Dostie J, et al. Gene expression during acute and prolonged hypoxia is regulated by distinct mechanisms of translational control. EMBO J 2006;25:1114–25.
6. Koumenis C, Naczki C, Koritzinsky M, Rastani S, Diehl A, Sonenberg N, et al. Regulation of protein synthesis by hypoxia via activation of the endoplasmic reticulum kinase PERK and phosphorylation of the translation initiation factor eIF2alpha. Mol Cell Biol 2002;22:7405–16.
7. Bi M, Naczki C, Koritzinsky M, Fels D, Blais J, Hu N, et al. ER stress-regulated translation increases tolerance to extreme hypoxia and promotes tumor growth. EMBO J 2005;24:3470–81.
8. Erler JT, Cawthorne CJ, Williams KJ, Koritzinsky M, Wouters BG, Wilson C, et al. Hypoxia-mediated down-regulation of Bid and Bax in tumors occurs via hypoxia-inducible factor 1-dependent and -independent mechanisms and contributes to drug resistance. Mol Cell Biol 2004;24:2875–89.
9. Lefebvre VH, Van Steenbrugge M, Beckers V, Roberfroid M, Buc-Calderon P. Adenine nucleotides and inhibition of protein synthesis in isolated hepatocytes incubated under different pO2 levels. Arch Biochem Biophys 1993;304:322–31.
10. Koritzinsky M, Levitin F, van den Beucken T, Rumantir RA, Harding NJ, Chu KC, et al. Two phases of disulfide bond formation have differing requirements for oxygen. J Cell Biol 2013;203:615–27.
11. Sonenberg N, Hinnebusch AG. Regulation of translation initiation in eukaryotes: mechanisms and biological targets. Cell 2009;136:731–45.
12. Proud CG. Signalling to translation: how signal transduction pathways control the protein synthetic machinery. Biochem J 2007;403:217–34.
13. Ayuso MI, Hernandez-Jimenez M, Martin ME, Salinas M, Alcazar A. New hierarchical phosphorylation pathway of the translational repressor eIF4E-binding protein 1 (4E-BP1) in ischemia-reperfusion stress. J Biol Chem 2010;285:34355–63.
14. Rousseau D, Gingras AC, Pause A, Sonenberg N. The eIF4E-binding proteins 1 and 2 are negative regulators of cell growth. Oncogene 1996;13:2415–20.
15. Martineau Y, Azar R, Bousquet C, Pyronnet S. Anti-oncogenic potential of the eIF4E-binding proteins. Oncogene 2013;32:671–7.
16. Browne GJ, Proud CG. A novel mTOR-regulated phosphorylation site in elongation factor 2 kinase modulates the activity of the kinase and its binding to calmodulin. Mol Cell Biol 2004;24:2986–97.
17. Saxton RA, Sabatini DM. mTOR Signaling in Growth, Metabolism, and Disease. Cell 2017;168:960–76.
18. De Benedetti A, Graff JR. eIF-4E expression and its role in malignancies and metastases. Oncogene 2004;23:3189–99.
19. Lazaris-Karatzas A, Montine KS, Sonenberg N. Malignant transformation by a eukaryotic initiation factor subunit that binds to mRNA 5′ cap. Nature 1990;345:544–7.
20. Wendel HG, De Stanchina E, Fridman JS, Malina A, Ray S, Kogan S, et al. Survival signalling by Akt and eIF4E in oncogenesis and cancer therapy. Nature 2004;428:332–7.
21. Graff JR, Konicek BW, Carter JH, Marcusson EG. Targeting the eukaryotic translation initiation factor 4E for cancer therapy. Cancer Res 2008;68:631–4.
22. Kong J, Lasko P. Translational control in cellular and developmental processes. Nat Rev Genet 2012;13:383–94.
23. Petroulakis E, Parsyan A, Dowling RJ, LeBacquer O, Martineau Y, Bidinosti M, et al. p53-dependent translational control of senescence and transformation via 4E-BPs. Cancer Cell 2009;16:439–46.
24. Rouschop KM, Dubois L, Schaaf MB, van den Beucken T, Lieuwes N, Keulers TG, et al. Deregulation of cap-dependent mRNA translation increases tumour radiosensitivity through reduction of the hypoxic fraction. Radiother Oncol 2011;99:385–91.
25. Trotman LC, Niki M, Dotan ZA, Koutcher JA, Di Cristofano A, Xiao A, et al. Pten dose dictates cancer progression in the prostate. PLoS Biol 2003;1:E59.

26. Le Bacquer O, Petroulakis E, Paglialunga S, Poulin F, Richard D, Cianflone K, et al. Elevated sensitivity to diet-induced obesity and insulin resistance in mice lacking 4E-BP1 and 4E-BP2. J Clin Invest 2007;117:387–96.
27. Evans SM, Joiner B, Jenkins WT, Laughlin KM, Lord EM, Koch CJ. Identification of hypoxia in cells and tissues of epigastric 9L rat glioma using EF5 [2-(2-nitro-1H-imidazol-1-yl)-N-(2,2,3,3,3-pentafluoropropyl) acetamide]. Br J Cancer 1995;72:875–82.
28. Ramaekers CH, van den Beucken T, Meng A, Kassam S, Thoms J, Bristow RG, et al. Hypoxia disrupts the Fanconi anemia pathway and sensitizes cells to chemotherapy through regulation of UBE2T. Radiother Oncol 2011; 101:190–7.
29. Rouschop KM, Ramaekers CH, Schaaf MB, Keulers TG, Savelkouls KG, Lambin P, et al. Autophagy is required during cycling hypoxia to lower production of reactive oxygen species. Radiother Oncol 2009; 92:411–6.
30. Pause A, Belsham GJ, Gingras AC, Donze O, Lin TA, Lawrence JC Jr., et al. Insulin-dependent stimulation of protein synthesis by phosphorylation of a regulator of 5′-cap function. Nature 1994;371:762–7.
31. Guo XN, Rajput A, Rose R, Hauser J, Beko A, Kuropatwinski K, et al. Mutant PIK3CA-bearing colon cancer cells display increased metastasis in an orthotopic model. Cancer Res 2007;67:5851–8.
32. Furic L, Rong L, Larsson O, Koumakpayi IH, Yoshida K, Brueschke A, et al. eIF4E phosphorylation promotes tumorigenesis and is associated with prostate cancer progression. Proc Natl Acad Sci U S A 2010; 107:14134–9.
33. Kim YY, Von Weymarn L, Larsson O, Fan D, Underwood JM, Peterson MS, et al. Eukaryotic initiation factor 4E binding protein family of proteins: sentinels at a translational control checkpoint in lung tumor defense. Cancer Res 2009;69:8455–62.
34. She QB, Halilovic E, Ye Q, Zhen W, Shirasawa S, Sasazuki T, et al. 4E-BP1 is a key effector of the oncogenic activation of the AKT and ERK signaling pathways that integrates their function in tumors. Cancer Cell 2010;18:39–51.
35. Poulin F, Brueschke A, Sonenberg N. Gene fusion and overlapping reading frames in the mammalian genes for 4E-BP3 and MASK. J Biol Chem 2003;278:52290–7.
36. Gingras AC, Raught B, Gygi SP, Niedzwiecka A, Miron M, Burley SK, et al. Hierarchical phosphorylation of the translation inhibitor 4E-BP1. Genes Dev 2001;15:2852–64.
37. Chen CC, Lee JC, Chang MC. 4E-BP3 regulates eIF4E-mediated nuclear mRNA export and interacts with replication protein A2. FEBS Lett 2012;586:2260–6.